Temperature dependence of luminescence efficiency, exciton transfer, and exciton localization in GaAs/$Al_xGa_{1-x}As$ quantum wires and quantum dots

Yong Zhang* and M. D. Sturge
Department of Physics and Astronomy, Dartmouth College, Hanover, New Hampshire 03755-3528

K. Kash
Department of Physics, Case Western Reserve University, Cleveland, Ohio 44106-7079

B. P. van der Gaag, A. S. Gozdz, L. T. Florez, and J. P. Harbison
Bellcore, Red Bank, New Jersey 07701-7040

(Received 11 August 1994; revised manuscript received 19 December 1994)

By studying the temperature dependence of the photoluminescence intensity in strain-confined GaAs/$Al_xGa_{1-x}As$ quantum wires and quantum dots, we show that as dimensionality is reduced from two-dimensional (2D) through 1D to 0D, there is no reduction of luminescent efficiency at low temperature, and that high quantum efficiency persists to significantly higher temperature. There is efficient spatial energy transfer from the 2D region to the 1D or 0D region. This transfer increases with temperature, showing that there is a barrier to transfer a few meV high. This barrier is lower than theoretically predicted. For above band-gap excitation there is substantial "capture transfer" in which unthermalized carriers or excitons transfer even at very low temperature. Exciton localization due to the well-width fluctuations of the host quantum well also plays an important role in determining the temperature dependence of the exciton transfer in these structures.

I. INTRODUCTION

In the past two decades, there has been a vast amount of work on semiconductor quantum wells, both experimentally and theoretically.[1] Interest in reduced dimensionality has been extended to semiconductor quantum wires and dots for more than a decade.[2,3] Existing techniques for generating significant lateral confinement to quantum wells are reviewed in Ref. 3. Among them, the following are most frequently used. (1) Patterned etching: this is perhaps the most direct method for making quantum wires and dots out of quantum wells.[4,5] (2) Ion implantation.[6] (3) Growth on nonplanar substrates: this technique gives better luminescence efficiency than etching and ion implantation.[7] However, the uniformity of samples depends very critically on the growth rate, which is difficult to control. (4) Strain confinement.[8,9] This method, proposed by Kash *et al.* is to put a so-called "stressor" on the top of a quantum well. The stressor deforms the quantum well locally and generates lateral confinement by lowering the band gap. This method can produce quantum wires and dots with high luminescent efficiency down to the scale of a few tens of nanometers. Growth methods that do not require patterning have also been developed. These include spinodal decomposition,[10] growth on self-organizing structures,[11] and strain-induced three-dimensional growth of islands.[12,13]

A wide variety of optical experiments has been carried out on these low-dimensional structures.[14–31] With one exception, these measurements were all made at low (helium) temperature. However, from the application point of view, the optical properties at higher temperature are more important, since nonradiative processes usually become significant with increasing temperature. Among the various techniques for making quantum wires and dots, strain patterning is perhaps the best for achieving high luminescent efficiency, making possible a meaningful comparison of the efficiency of wells, wires, and dots. The efficiency of our strain confined quantum wires and dots is not only comparable to that of the host quantum wells at low temperature,[28] but also persists to relatively high temperature, as we briefly reported recently.[29,30] As the dimensionality is reduced from 2D through 1D to 0D, the temperature dependence of the nonradiative and radiative decay, and of electron-phonon interaction, all change. As far as we know, the only other systematic investigation of the temperature dependence of the luminescence efficiency and luminescence decay time was made on strain-induced three-dimensional islands,[31] whose geometry and composition were not yet precisely known. An important issue in such structures is carrier or exciton localization, since interface imperfections are unavoidable. In the low-temperature limit, localization causes a Stokes shift[21] and affects the free-exciton radiative decay time.[30] However, its role at finite temperature is not clear yet.

In this paper, we study the temperature dependence of the luminescence in strain-confined quantum wires and quantum dots. Section II describes the quantum wire and dot structures, their strain tensors, and the experimental setup. Section III reports steady-state measurements of the temperature dependence of luminescence in quantum wires and dots of various sizes, with comparison to unpatterned quantum wells. The main results of this section are (1) as dimensionality is reduced from 2D through 1D to 0D, nonradiative recombination is effectively re-

duced and thus higher quantum efficiency is achieved at relatively high temperature; (2) there is efficient, but temperature-dependent, spatial energy transfer from the 2D region, across a strain induced barrier, to the 1D or 0D region. In Sec. IV, we discuss the influence of energy relaxation of hot carriers or excitons in quantum wires and dots on the luminescent efficiency. We use a kinetic model to obtain the effective transfer rate and compare it with the theoretical prediction. Finally, in Sec. V, we summarize this work and give some conclusions.

II. SAMPLES AND EXPERIMENTAL SETUP

A. Samples

The details of the fabrication of the strain-confining structures have been described elsewhere.[32] Briefly, radio-frequency plasma deposition employing butane as the carbon-containing gas was used to put down a 100–300 nm-thick, uniform layer of amorphous hydrogenated carbon (*a*-C:H) onto a quantum-well sample. The bonding defects created by the impact of high-energy ions during growth of the film produce stress in the carbon film. The carbon layer is patterned by electron-beam lithography and etched. Upon etching, the carbon wires or dots ("stressors") left on the sample expand, and in their partial relaxation, they locally deform the underlying quantum well.

This work concentrates on two samples, *A* and *B*, grown by molecular-beam epitaxy (MBE) on [100] oriented semi-insulating GaAs. Sample *A* has three GaAs wells of 9, 2, and 4 nm thickness, separated by 20 nm thick $Al_{0.3}Ga_{0.7}As$ barriers, and a 30-nm cap layer. Onto this structure, a 160 nm thick *a*-C:H layer was patterned and etched to form 40–50-μm square arrays of works along the [100] direction. There are two arrays of wires in this sample, labeled *W*2 and *W*3. *W*2 and *W*3 have wires 350 nm wide (measured by scanning electron microscopy), and period 1 and 2 μm, respectively. We will use symbol *A*-*W*3 (350/9 nm) for the spectra of the 9-nm QW in the 350-nm array *W*3 of sample *A*, and so on.

Sample *B* was grown in the following sequence: 500-nm GaAs buffer layer, a 200-nm barrier layer consisting of 160 nm of $Al_{0.3}Ga_{0.7}As$, followed by a twenty layer superlattice of 1.4 nm of GaAs and 0.6-nm AlAs (with the same average composition as $Al_{0.3}Ga_{0.7}As$), inserted to smooth the lower interface and to trap impurities, a 12-nm quantum well, a 20-nm barrier of $Al_{0.3}Ga_{0.7}As$, and a 30-nm GaAs cap layer. A 100-nm *a*-C:H layer was deposited, patterned, and etched to form 40-μm square arrays of stressor wires or dots. The wires are along the [100] direction, while the dots are squares with sides in the same orientation. The wires or dots with nominal stressor sizes 100, 200, 300, 400, and 800 nm were made in this sample, and they are labeled *B*-*W*1 (100/12 nm); *B*-*W*5 (800/12 nm) or *B*-*D*1 (100/12 nm); *B*-*D*5 (800/12 nm), respectively. The periods are three times the nominal sizes.

B. Strain tensors and band structure

The strain tensors are calculated as described previously.[17] A typical contour plot of the strain is shown in Fig. 1. The material under the center of the stressor is dilated; that near the edges is compressed. The decay length of the strain is comparable to the width of the stressor, regardless of the details of its structure, so the quantum well must be located as close as possible to the stressor in order to get strong band-gap modulation. However, it cannot be less than about 50 nm from the stressor, because interface states adversely affect the luminescent efficiency. Since the deformation potential is negative, a potential well for electrons is created in the region of the well under the stressor, while barriers are formed near the edges, as shown for two wire widths in Fig. 2. Near the minimum, the potential is parabolic, and the electron energy-level spacing is about 2.5 meV in the 200-nm case and 1 meV in the 350-nm case. The effect on the valence band is more complicated because of the off-diagonal components associated with shear strain[17,32,33] (which are not shown in Fig. 1), and depends on the details of the geometry (see Fig. 10 below for a particular case).

C. Experimental setup

Most of the nonselective luminescence spectra were excited with a He-Ne laser. This was focused to a measured spot diameter at 12 μm, compared with the pattern size of 40 μm. Selective luminescence spectra and photoluminescence excitation (PLE) spectra were obtained with a cw dye laser using LDS 751 dye. The spot diameter was $\sim$20 μm in this case. The laser spot was focused centrally on the patterns and was checked with a microscope ($\times$20). However, some laser light always reached the unpatterned region, particularly in the case of selective excitation.

The sample was cooled by helium gas in a variable temperature cryostat. A thermocouple was attached to the sample holder at the same height as the sample to measure temperature, which was stabilized by a heater in the

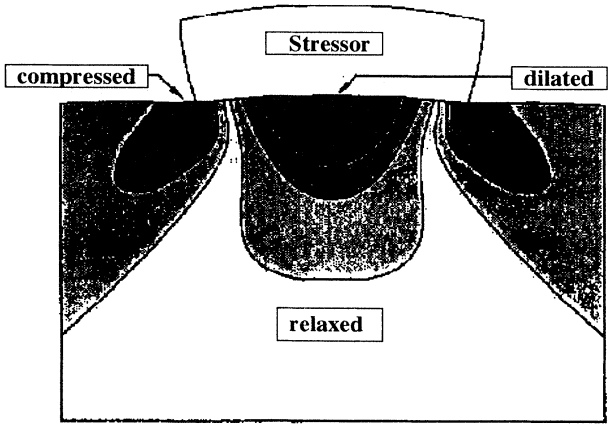

FIG. 1. Contour plot of volume dilatation of semiconductor. Contours are at equal intervals of the dilatation. The deformation is exaggerated.

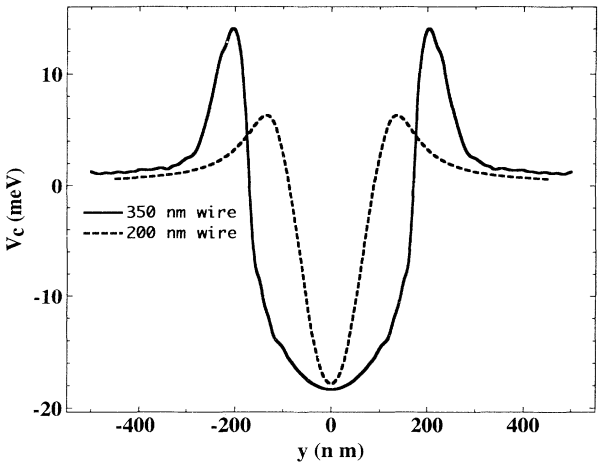

FIG. 2. Calculated modulation of the conduction-band edge by inhomogeneous strain, for two stressor widths.

dewar and an external temperature controller (Air Product Model 3700-APC) in the range of about 2 to 80 K with an accuracy of about ± 0.1 K.

The luminescence signal was dispersed through a 1-m double grating monochromator (Spex Industries Model 1400 II). Typically, a 0.3-mm slit width ($\delta\lambda = 2$ Å) was used. A Hamamatsu R636 PMT (GaAs cathode) was used for these cw measurements (time-resolved measurements, using a multichannel plate tube will be reported elsewhere). The DC signal from the PMT was amplified, converted to digital form and recorded in a computer.

III. EXPERIMENTAL RESULTS

A. Low-temperature results

In this subsection, we report the luminescence and PLE spectra of the strain-confined structures, and show that at low temperature the luminescence efficiencies of quantum wires and quantum dots are comparable to that of their host quantum wells. We discuss how excitons transfer to quantum wires and dots and how the transfer affects the luminescence in these structures.

Since the quantum wire (QWW) and quantum dot (QWD) structures were made by strain patterning previously grown quantum well (QW) structures, the quality of the QW affects the properties of the QWW's and QWD's. In general, interface roughness of QW's introduces inhomogeneous broadening of the exciton peak.[34] At liquid-helium temperature (~ 4 K) and with excitation density ~ 20 W/cm^2, the full width at half maximum (FWHM) of the heavy-hole exciton for the unpatterned QW's in sample A are the following: ~ 5 meV for the 9-nm QW, ~ 6 meV for the 4-nm QW, and ~ 8.5 meV for the 2-nm QW; for sample B (12 nm) it is ~ 4 meV. In terms of interface roughness, these two samples are not among the best which have been reported.[35] However, the internal quantum efficiency appears to be about 100% at low temperature.

In general, a nonresonantly excited strain confined quantum wire has two major peaks in its luminescence spectrum: "HH"—the heavy-hole exciton peak from QW in the unstrained region between wires (and, if focusing is imperfect, from the unpatterned region) and "HHW"—the heavy-hole exciton peak from QWW. Figure 3 is the luminescence spectrum of A-$W3$ (350 nm). There is a set of HH and HHW lines for each of the three strained QW's. The "EW" line in Fig. 3 is from excitons in a quantum wire formed at the interface of the lowest $A_xGa_{1-x}As$ barrier/GaAs buffer layer, which is discussed elsewhere.[36] Since EW is from a region separated from the unstrained QW by a thick barrier, there is no communication between the QW and EW, that is, excitons in the QW to not transfer to the EW.

The intensity ratio of HH to HHW is sensitive to the tightness of focusing and to the accuracy of positioning the laser spot on the patterned region. However, for the two 350-nm wire arrays, A-$W2$ (350 nm) and A-$W3$ (350 nm) the total intensity of HH plus HHW is nearly constant, showing that the luminescent efficiencies of QW and QWW are the same, i.e., the strain patterning does not introduce extra nonradiative decay. The spectrum for another array, $W2$ (350 nm), in sample A is similar to Fig. 3, but the HH to HHW intensity ratio is different, due to the different "geometric ratio," i.e., the ratio of the patterned wire width to the wire separation.

The excitation-density dependence of the HH and HHW intensities has been measured. For both of them a linear dependence is found from 1 to 8×10^3 W/cm^2. This work will concentrate on this linear region.

The geometric ratio is 0.54 for $W2$ and 0.21 for $W3$, but the HHW/HH ratio is much larger than this, as can be seen clearly in Fig. 3. This is because excitons created between the wires can transfer directly to the wires.[28] If there were no transfer, the ratio of the luminescence would be closer to the geometric ratio,[37] so long as the laser spot is focused within the patterned area. On the other hand, if there were no potential barriers at the

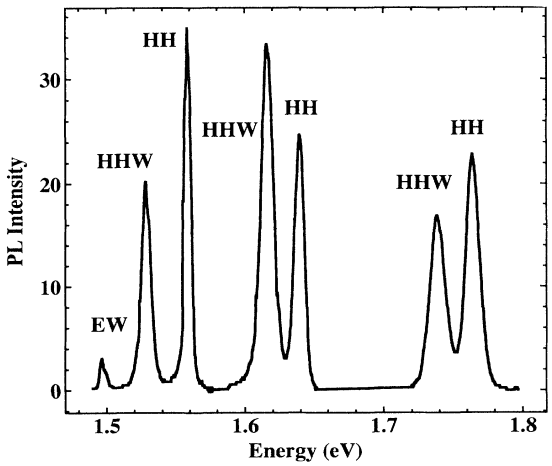

FIG. 3. Photoluminescence spectrum of an array of 350-nm wires, $W3$, in sample A. There are three sets of (HH,HHW) lines, associated with three strained quantum wells with well width 9, 4, and 2 nm. The integrated intensity ratios of HHW to HH are 0.58, 0.74, and 1.35 for the 9-, 2-, and 4-nm quantum wells, respectively.

edges of the wires, most of the excitons created between the wires would transfer to the wires before they decay radiatively, as in the case of the so-called *V*-groove quantum wires.[7] The relative intensity of the HH and HHW varies for the three QW's at different depths beneath the stressor, as shown in Fig. 3, which indicates that the transfer efficiency is different for each QW. The 4-nm QW has the lowest barriers since it is the one farthest from the stressor, and as expected, the HHW/HH ratio is largest for this QW.

The PLE spectrum of the HHW of *A-W*3 (350/9 nm) was measured. While no structure attributable to QWW subbands could be resolved, two PLE peaks corresponding to the light- and heavy-hole exciton states in the QW could be clearly seen, indicating some tunneling transfer from the interwire region to the wires. Their peak positions are blueshifted by 2–4 meV from the unpatterned QW. This shift has been observed before and was attributed to excitons in the slightly compressed QW regions between stressors.[28] Another possible explanation is that the PLE intensity is a convolution of the absorption spectrum of the QW exciton and the tunneling rate. Such a combined effect will lead to the blueshift of the PLE peaks since tunneling increases with increasing energy.

The QW peaks in the PLE are weak relative to direct excitation into the wire, showing that the contribution of transfer from low-lying QW states is much smaller than that of direct excitation of QWW states. When the excitation energy is near HH, the transfer contribution is less than 20% of the total. However, in luminescence spectra obtained with well above band-gap excitation, for instance Fig. 3, the contribution of transfer is nearly 50% of the total HHW integrated intensity. Thus, transfer is more efficient at high excitation energy. This result implies that the transfer is taking place, while carriers or excitons are still hot. We distinguish between three transfer processes, illustrated in Fig. 4. These are *capture transfer,* in which carriers or excitons created in the interwire region are captured into the wire when their energy is higher than the barrier, *tunneling transfer,* which occurs when the exciton energy is lower than the barrier height, and classical *activation transfer,* due to thermal activation across the barrier, which is negligible at the low temperatures considered in this section. The closer to the bottom of the barrier, the more difficult it is to tunnel through the barrier. It will be even more difficult if the excitons relax to localized exciton states in the QW. Figure 4 includes these localized states, which are discussed later.

Figure 5 shows the nonresonantly excited luminescence spectra of all the wires and dots in sample *B*, with comparison to the unpatterned QW. "HHD" is the HH hole exciton peak from QWD. The redshift of HHD, with respect to HH, is larger than HHW for the same stressor size, since in this case $\varepsilon_{xx} \neq 0$. In sample *B*, in which the geometric ratio is ~ 0.5 for wires and 0.125 for dots, HHW or HHD is stronger than HH for above band-gap excitation.[37] There is clearly strong transfer from the interwire or interdot region to wires or dots. There are some extra peaks in these spectra, whose origin is obscure. Possible explanations are discussed in Ref. 38.

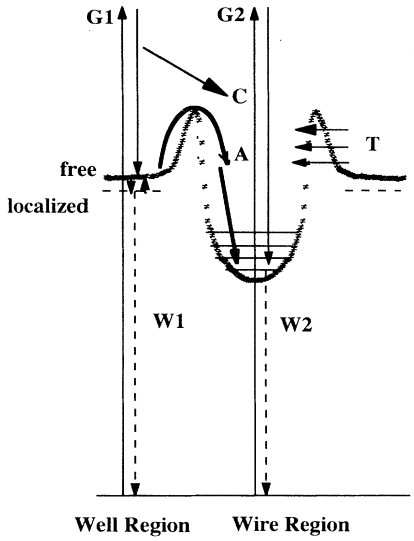

FIG. 4. Exciton generation and transfer in a quantum wire structure with above band-gap excitation. G_1 and G_2 stand for initial generation rates of nonthermal excitons, w_1 and w_2 for radiative recombination rates of free or localized excitons in well and wire regions, respectively. *C* stands for capture transfer, *A* for thermal activation transfer, and *T* for tunneling transfer from well region to wire region.

B. High-temperature results

In this subsection, we will show that the high quantum efficiency obtained at low temperature for QWW's and QWD's persists to significant by higher temperature than

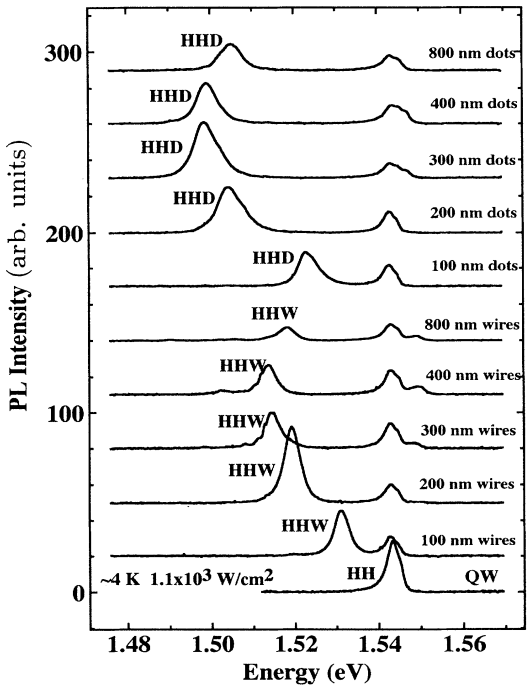

FIG. 5. Photoluminescence spectra of all wires and dots in sample *B*, compared to the unpatterned QW (bottom curve).

that of the unpatterned QW's, and that energy transfer from the QW to QWW and QWD is thermally enhanced. The mechanisms for the thermal enhancement will be discussed.

In a bulk (3D) semiconductor, nonradiative decay of excitons, due to diffusion of excitons to nonradiative centers, tends to dominate the luminescence and increases with increasing temperature. In a QW (quasi-two-dimensional) spatial confinement reduces the ability of excitons to reach nonradiative centers and raises the luminescence efficiency, especially at low temperature, where the excitons are localized. This effect of spatial confinement should increase further when the dimensionality is reduced to quasi-one-dimensional or quasi-zero-dimensional. However, although many QWW or QWD structures have been investigated, there has not to date been any systematic comparison of the temperature dependence of the luminescence efficiency of QWW's and QWD's with QW's of known comparable quality. Strain confinement is unique in that extra nonradiative centers are not introduced during fabrication. We will show that these strain confined QWW's and QWD's are indeed better than their host QW's in suppressing nonradiative recombination.

Figures 6(a) and 6(b) show the temperature variation of the integrated luminescence intensities and the corresponding luminescence spectra for *A-W*3 (350/9 nm) at a low excitation density (80 W/cm^2). The small wavelength shifts as the temperature is raised are due to delocalization of the exciton (an initial blueshift) followed a redshift, due to the decreasing band gap. We concentrate here on the integrated intensity. Figure 7 shows the corresponding temperature variation for *A-W*3 (350/2 nm). The results for the unpatterned QW's with the same excitation density are also included for comparison. The common feature in these structures is that while the QW emission quenches faster than in the unpatterned QW's with increasing temperature, the QWW emission increases and the total QW + QWW intensity remains nearly constant up to 60 or 80 K, where the luminescence of the unpatterned QW has quenched substantially. With increasing temperature, more excitation energy is transferred from the interwire region to the wires with little nonradiative loss. There is less nonradiative recombination within the wires than in the unpatterned QW's, and the transfer process dominates the nonradiative process in the interwire QW. A more detailed discussion of the temperature dependence of the luminescence intensities, with an explanation of the lines in Fig. 7(a), will be given in the next section. Similar results are also obtained for another array, *A-W*2 (350 nm).

Figure 8 shows the temperature dependence of the QWW luminescence of *A-W*3 (350/9 nm) obtained with excitation resonant with HH. The excitation power is about 40 times that used in Fig. 6, but because the absorption is weaker at the longer laser wavelength and the dye laser could not be focused as tightly as the He-Ne laser, the carrier density is only about 5 times higher. Comparison of Figs. 6(a) and 8 clearly shows the distinction between capture transfer, which is only present for above band-gap excitation and is weakly (if at all) dependent on temperature, and the strongly temperature-dependent activation transfer. Quenching, due to nonradiative decay, starts at about 50 K in Fig. 8, and is more significant than in the case of nonresonant excitation, because cold excitons in the QW have more of a chance to recombine nonradiatively before they transfer to the wires than do the hot excitons responsible for capture transfer.

Referring to Fig. 4, we see that there are several contributions to the temperature dependence of the transfer rate besides thermal activation over the barrier (activa-

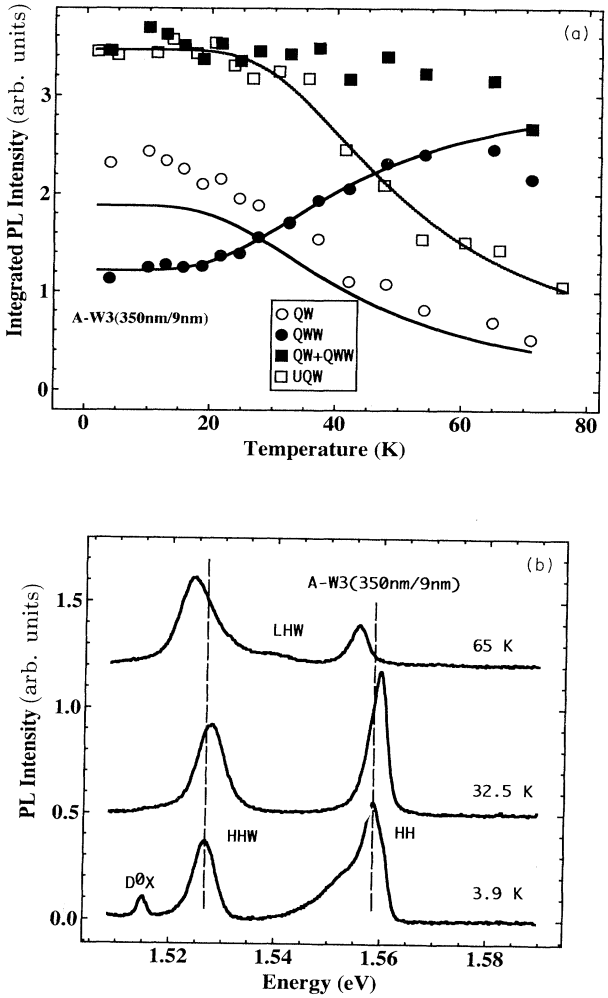

FIG. 6. (a) Integrated photoluminescence intensities versus temperature for *A-W*3 (350/9 nm), compared to the unpatterned 9-nm quantum well. Filled circles—quantum wires (QWW); open circles—quantum well in the interwire region (QW); filled squares—sum of QW and QWW; open squares—unpatterned QW (UQW). Excitation 80 W/cm^2 at 1.96 eV. Solid lines are fitted theoretical curves from the kinetic model of Sec. IV. The line through the UQW data is a guide to the eye. (b) Photoluminescence spectra of *A-W*3 (350/9 nm) at various temperatures. As the temperature is raised, the excitons delocalize and the lines shift initially to higher energy, but at a higher temperature the band gap decreases, shifting the lines to lower energy.

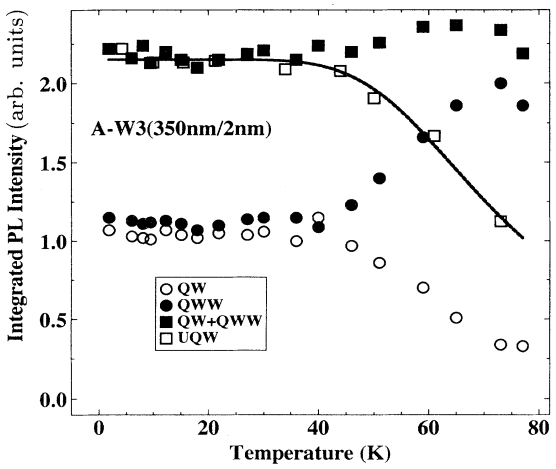

FIG. 7. Same as Fig. 6(a), for sample *A-W*3 (350/2 nm).

tion transfer). (1) Tunneling transfer will also be enhanced because a thermally excited exciton sees a lower and thinner barrier. However, this cannot be distinguished experimentally from activation transfer, and the calculation[38] shows that the correction due to this is small in the relevant temperature range. (2) Thermalization of QW excitons increases the exciton decay time,[36] so that more excitons or carriers can transfer to the wire within their lifetime. (3) Thermal activation of localized excitons in the QW: free-excitons transfer more easily to the wire.

These mechanisms coexist in the observed thermal enhancement of the transfer. If the temperature dependence of activation transfer were dominant, thermal enhancement would have occurred at a lower temperature in *A-W*3 (350/2 nm) than in *A-W*3 (350/9 nm), since the former QW has a lower barrier, being further from the stressor. This is contrary to the experimental results. Therefore, the other two mechanisms must play a role, in particular the third, the 2-nm QW having a larger localization energy.

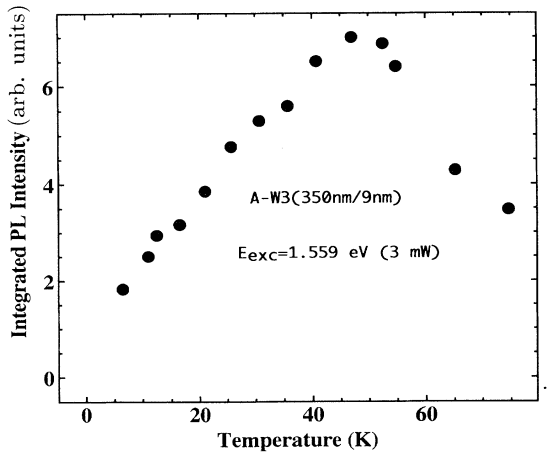

FIG. 8. Integrated photoluminescence intensity of quantum wires versus temperature with resonant excitation to the heavy-hole exciton state of the quantum well for *A-W*3 (350/9 nm).

By comparing the geometric ratio to the actual HHW/HH intensity ratio at low temperature, one can estimate the transfer contribution in the HHW. For instance, from the data on HHW in *A-W*3 (350/9 nm) (Fig. 6), the transfer contribution is ~47%. On the other hand, if we assume that the contribution of direct excitation into the wire is temperature independent and take the contribution of the tunneling transfer at low temperature to be 20% (estimated from the PLE spectrum: see above), the resonance excitation data (Fig. 8) show that activation transfer increases by a factor of about 16 at ~50 K. Furthermore, if the total transfer contribution for nonselective excitation is treated as the sum of activation plus tunneling from the HH states and capture from higher-lying states, and if the contributions of capture transfer and direct excitation are assumed to be temperature independent, one can combine the information given by the results of the above band-gap excitation [Fig. 6(a)] and selective excitation (Fig. 8) to obtain the contributions from each mechanism. With above band-gap excitation at low temperature, this analysis indicates that ~53% of the HHW comes from direct excitation, ~39% from capture transfer, and ~8% from tunneling transfer for *A-W*3 (350/9 nm). The tunneling probability, i.e., the fraction of fully relaxed HH excitons tunneling to the wire, is ~4% for *A-W*3 (350/9 nm). The different contributions depend on the geometric ratio. For *A-W*2 (350/9 nm), which has a larger geometric ratio, they are ~56% (direct excitation), ~42% (capture), and ~2% (tunneling). The above analysis shows that tunneling transfer is usually small at low temperature, but that activation transfer is greatly enhanced at high temperature. The fact that the contribution of "capture" transfer is essentially the same for *A-W*2 and *A-W*3, whose geometric ratios differ by a factor of 2.5, shows that nonradiative decay in the quantum well (as opposed to the wire) is not important for the hot excitons involved in this process, whereas the lower "tunneling" contribution for the sample with smaller geometric ratio shows that it is important for thermalized excitons.

These CW results are supported by transient measurements. At low temperature, the luminescence decay time of the QW excitons is not affected by patterning, because of the small tunneling rate. As temperature increases, the luminescence decay time of HH in a patterned QW becomes significantly shorter than in an unpatterned QW, while the rise time of HHW increases, due to an increasing contribution of the relatively slow exciton transfer from the interwire region to the wire region. The transient results are discussed in detail elsewhere.[30,38,48]

Qualitatively, the temperature dependence of luminescence intensity in QWD's is similar to that in QWW's. However, QWD's suppress nonradiative processes even more efficiently than QWW's. For example, Figs. 9(a)–9(c) show the temperature dependence of the integrated QWD intensities for *B-D*2 (200/12 nm), *B-D*4 (400/12 nm), and *B-D*5 (800/12 nm). The temperature dependence for the 12-nm unpatterned QW is also shown in the plots, scaled to the total intensity at 4 K. The total intensity QW plus QWD is approximately constant up to a temperature well above the quenching temperature for

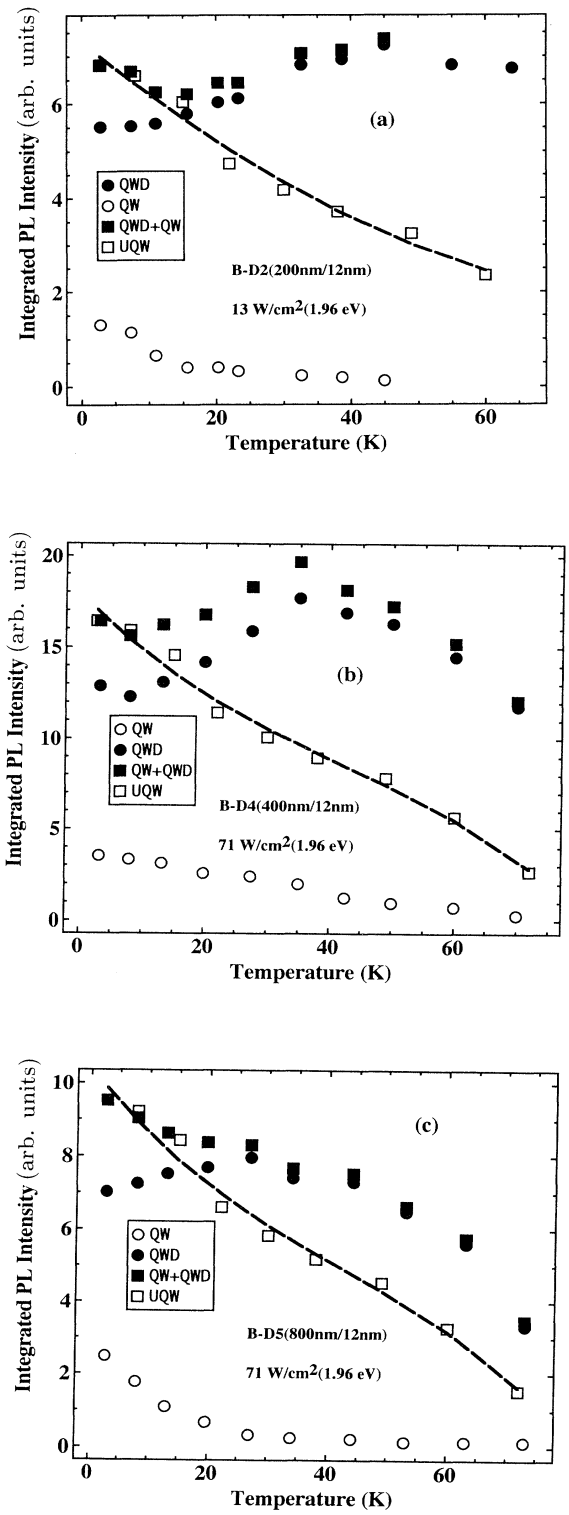

FIG. 9. (a) Integrated photoluminescence intensities versus temperature for quantum dots. (a) *B-D*2 (100/12 nm), (b) *B-D*4 (400/12 nm), and (c) *B-D*5 (800/12 nm) compared to the unpatterned 12-nm quantum well. Filled circles—quantum dots (QWD); open circles—QW in the interdot region; filled squares—sum of QW and QWD; open squares—unpatterned QW.

the unpatterned QW. There may even be a small increase of the total intensity, due to the competition of thermally enhanced transfer with nonradiative processes in the QW. The quenching temperature increases as dot size is reduced, showing that the suppression of nonradiative decay is stronger for smaller confinement size. Even at 150 K, the luminescence efficiency of the patterned structures is about twice that of the parent unpatterned QW. This suppression of nonradiative recombination could be an important feature for possible applications of these quantum structures.

IV. DISCUSSION

A. Luminescence efficiency and carrier relaxation in quantum wires and quantum dots

The luminescence efficiency is determined by the competition between radiative and nonradiative recombination. We will now discuss the influence of reduced dimensionality on this competition.

First, we consider how the lateral confinement of quantum wires and dots affects the competition between radiative and nonradiative recombination at the luminescent states. Very little is known about the origin of nonradiative decay in $GaAs/Al_xGa_{1-x}As$ quantum wells. Nonradiative processes, in general, are not well understood, and the uncontrolled variation in samples from different sources makes it hard to draw general conclusions. In the host quantum wells, it is clear that migration to nonradiative centers leads to thermal quenching of luminescence although the microscopic mechanisms for the nonradiative processes may not be known. In quantum wires and quantum dots, lateral confinement reduces the probability that photogenerated particles (electrons, holes, or excitons) reach nonradiative centers. Our data show that lateral confinement by strain does not change the density of nonradiative centers, but it does change the spatial distribution and mobility of photogenerated particles. Because of lateral transfer, excitons which would be uniformly distributed in a larger 2D area without lateral confinement will be concentrated into the smaller wire or dot area. After relatively fast relaxation within the wire or dot, the excitons will be confined to a small region near the center of the wire or dot. The scale of this region is determined by the extension a_c of the ground-state wave function of the center-of-mass (COM) motion. (Here $2a_c$ is the FWHM of $|\psi|^2$, and in all cases considered here $a_c \gg a_B$, the exciton Bohr radius. COM motion of the exciton will be further discussed in the next subsection.) Well width fluctuations localize the excitons and we can define a length $a_{\rm loc}$ over which the variation of the lateral confinement potential is comparable to the localization energy. If $a_{\rm loc} > a_c$, the localization energy is larger than the wire or dot confinement energy and the excitons will be distributed over a distance $\sim a_{\rm loc}$, as in the QW. However, when the temperature is raised, the excitons will find it difficult to escape this region because of the lateral confinement, and nonradiative decay will be suppressed so long as $a_{\rm loc}$ is small compared with the diffusion length L_D of a free exciton in the QW ($L_D \sim 1$

μm). For example, in a typical 200-nm wire like *B-W2* (200/12 nm), a_c is calculated to be 12 nm,[38] and $a_{\rm loc} \sim 40$ nm (taking the localization energy to be of the order of the linewidth, say 5 meV). The number of accessible nonradiative centers in the wire is thus reduced, relative to the QW, by a factor $a_{\rm loc}/L_D \sim 1/25$. This effect will be even more pronounced in a dot. The same mechanism explains the suppression of impurity luminescence in quantum dots.[19]

We also need to consider excitons created in the QW. So long as the diffusion length in the QW is greater than half the interwire or interdot spacing, excitons delocalized by increasing temperature will transfer to the wire or dot before they find a nonradiative center in the QW, thus keeping the total luminescence intensity nearly constant up to significantly higher temperatures than in unpatterned QW's.

When excitons are nonresonantly excited, nonradiative recombination can occur during the cooling of the hot excitons. In a 1D or 0D system with 100–200-nm infinite high square-well potentials, intersubband electron relaxation by acoustic-phonon-electron scattering should be slow compared to relaxation in 3D and 2D systems at low temperature.[39] It has, therefore, been suggested[40] that the observed low luminescence efficiency of etched wires or dots[41–44] is an intrinsic effect rather than due to etch damage as usually believed. According to Ref. 40, this slow relaxation can increase the electron lifetime in an excited subband to tens of nanoseconds, longer than the usual nonradiative decay times in a 2D system. Furthermore, due to larger hole effective mass and smaller quantization energies, the thermalization of holes should be faster than that of electrons. Since band to band recombination of hot electrons with cold holes is forbidden by momentum conservation, low luminescence efficiency was predicted. However, the observed drastic reduction in the luminescent decay time[45,46] of etched wires and dots compared to unetched ones shows that nonradiative decay, due to etch damage, plays an important role in reducing the efficiency, whether carrier relaxation is slow or not. Furthermore, it has been pointed out[47] that the theory of Ref. 40 may anyway be inapplicable to excitons: the exciton-phonon-scattering rate can be significantly larger than the electron-phonon rate, because of electron-hole correlation. Our data show that when there is no surface damage the luminescence efficiency is no lower than that in the 2D case, even in our narrowest wires. Furthermore, time-resolved measurements on our samples show no indication of slow relaxation,[48] contrary to the prediction of Ref. 40 for a comparable sized wire. However, the lateral potential profile, and therefore the band structure (especially in the valence band), is quite different in our samples from the discontinuous profile considered in Ref. 40, so we cannot say for certain that our results contradict that prediction.

B. Thermally enhanced exciton transfer from quantum well to quantum wires and quantum dots

As shown in Sec. III, the excitons generated in the interwire or interdot region will transfer to the wires or dots by capture, activation, and tunneling transfer. The exciton generation and transfer processes in QWW or QWD structures are shown schematically in Fig. 4. We assume that capture transfer is temperature independent, so that the thermal enhancement is due to activation transfer of those excitons which relax to the bottom of the conduction band in the well. In the following, we consider the thermally enhanced transfer, due to these two mechanisms. For definiteness, the discussion will be restricted to quantum wires, but it applies qualitatively to quantum dots as well.

In the WKB approximation, the transmission coefficient, defined as the ratio of the transmitted current to the incident current, is given by[49–51]

$$T(E) \approx \exp\left[-\frac{2}{\hbar}\int_{y_1}^{y_2}\sqrt{2M[V(y)-E]}\,dy\right] . \tag{1}$$

Here, $V(y)$ is the lateral confinement potential for excitons in a wire, y_1 and y_2 are turning points where $V=E$, E is the exciton energy measured from the bottom of the excitonic band of the unstrained quantum well, and M is the mass of the quantum-well exciton.

Although we know the lateral confinement potentials for the electron and hole separately,[33] it is not trivial to construct a potential for the exciton. It is well known that the diffusion of free excitons is limited by the diffusion of the hole, since the hole has much larger effective mass, and thus much smaller mobility than the electron. (Electron-hole correlation affects the diffusion of the excitons, but only weakly.) In fact, the diffusion constant of free excitons[52] is of the same order as that of free holes and about an order of magnitude smaller than that of free electrons[53] in GaAs/$Al_xGa_{1-x}As$ quantum wells. In the quantum wire structure, the electron encounters a thick barrier, while there is usually no barrier for the (heavy) hole.[33] Obviously, the spatial transfer of the exciton will be determined by neither the electron nor the hole alone, and their correlation is important.

The effect of lateral strain confinement is analogous to that of well width fluctuations in quantum wells. Typically, the confinement potential in a strain-confined quantum wire is significantly larger than the fluctuation potential in a quantum well, but is still about an order of magnitude smaller than the typical quantum-well confinement potentials, and its scale is usually much larger than the width of the quantum well or the exciton radius. Thus, at least approximately, the quantum wire potential can be treated in the same way as the fluctuation potential from which the effective potential for the COM motion of an exciton can be obtained.[54] Accordingly, the effective potential for the COM motion of an exciton in the quantum wire or dot structure is

$$V(\mathbf{R}) = \int |\varphi(\mathbf{r})|^2 \left[V_e\left(\mathbf{R}+\frac{m_h}{M}\mathbf{r}\right) + V_h\left(\mathbf{R}-\frac{m_e}{M}\mathbf{r}\right)\right] d\mathbf{r} , \tag{2}$$

where $\varphi(\mathbf{r})$ is the envelope function, which describes the relative motion of the electron and hole in a quantum

well, V_e and V_h are the confinement potentials for the electron and hole, respectively. $\mathbf{r}=\mathbf{r}_e-\mathbf{r}_h$ is the relative coordinate, $\mathbf{R}=(m_e\mathbf{r}_e+m_h\mathbf{r}_h)/M$ the COM coordinate, and $M=m_e+m_h$. When the spatial variation of V_e and V_h is much slower than that of $\varphi(\mathbf{r}), |\varphi(\mathbf{r})|^2$ can be taken as a δ function and

$$V(\mathbf{R})=V_e(\mathbf{R})+V_h(\mathbf{R}) . \tag{3}$$

This result has been used to calculate the confinement potential of excitons in quantum wires[55] and COM quantization in wide II-VI quantum wells.[56] For strain-confined quantum wires and dots, the barrier thickness is of the order of 100 nm, the exciton Bohr radius is around 10 nm, and this approximation that we adopt is quite reasonable. The exact calculation using (2) will be left for future work. Strictly speaking, V_h should be a 4×4 matrix, due to the complicated valence-band structure.[33]

The confinement potential for COM motion for the 350-nm wires in sample A is shown in Fig. 10, according to Eq. 3. V_e and V_h are calculated by the method of Ref. 33 from the known strain tensor.[55] The calculated transmission coefficient for this barrier for $M=0.25m_0$,[57] can be approximated by $T(E)\approx\exp[-a(E_B-E)]$, where $a=4$ meV^{-1} and E_B is the barrier height. T is only significant within 1–2 meV of the barrier height, because the barrier is thick. Thus,

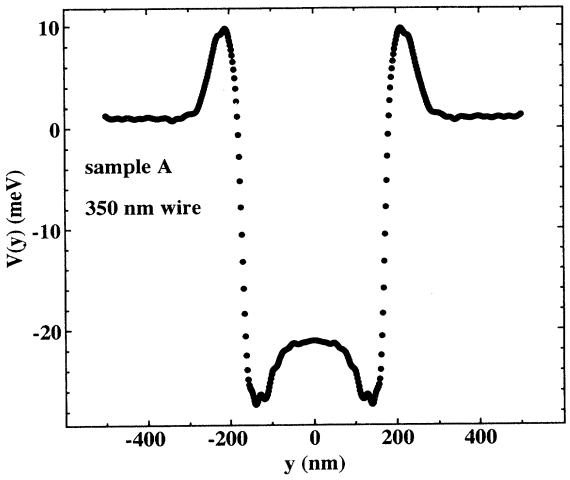

FIG. 10. Lateral confinement potential for exciton center-of-mass motion for the 350-nm quantum wire in sample A.

the temperature dependence of tunneling transfer is not distinguishable from that of classical activation transfer.

Assuming a Maxwell-Boltzmann distribution for the thermalized excitons, the total transmission coefficient is given by

$$P(T)=\frac{\int_0^{v_0}T(E)\rho(E)\exp(-E/k_BT)dE+\int_{v_0}^{\infty}\rho(E)\exp(-E/k_BT)dE}{\int_0^{\infty}\rho(E)\exp(-E/k_BT)dE} , \tag{4}$$

where $\rho(E)$ is the density of states and V_0 is the barrier height. The first term on the right-hand side is the contribution of thermally assisted tunneling, the second is the classical ("activation") term. The contribution of tunneling turns out to be negligible, and for a 2D system with a parabolic band structure, we have $P(T)=\exp(-V_0/k_BT)$.

We can now calculate the rate of transfer into the wire, w_t. If the area density of excitons in the 2D region is n, and they are in thermal equilibrium, the number of excitons striking the barrier per unit time and per unit wire length is given classically by $n\bar{v}/4$, where $\bar{v}=(8k_BT/\pi M)^{1/2}$ ($1.24\times10^6\sqrt{T}$ cm/s) is the average thermal velocity of excitons. Excitons enter the wire through two barriers, so the number of excitons transferring to the wire per unit time per unit wire length is $P(T)n\bar{v}/2$. Hence $w_t=P(T)\bar{v}/2L$, where L is the width of the 2D region.

The calculated transfer rate w_t for A-$W3$ (350/9 nm) with $L=1650$ nm is shown in Fig. 11. At high temperature, the calculated transfer rate is of the same order as the rate obtained from fitting to steady-state luminescence (see below), and considering the relatively large experimental error and approximations made in the theoretical model, the agreement at high temperatures is reasonable. On the other hand, at low temperatures, the transfer rate should be practically zero, but it is quite appreciable according to the PLE. One possible explanation is that the tunneling has been treated as a single barrier problem in above calculation. Due to the double barrier structure of the wire, there are some quasibound states,[38] which have energies near or above the ground state of the quantum-well exciton. Resonant tunneling could significantly enhance the transfer at low temperature. Another possibility is that, at some places along the wire, due to the fluctuation of the QW width, the barrier

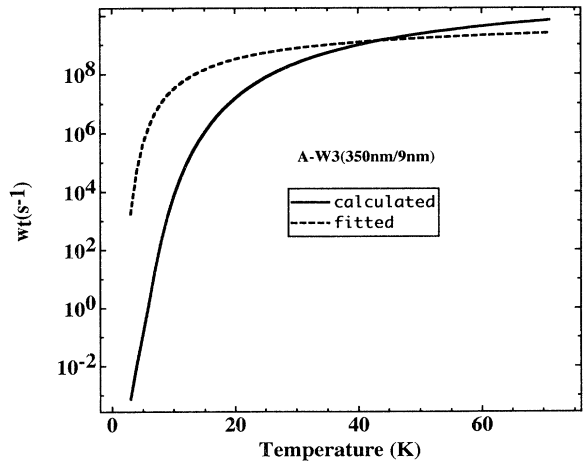

FIG. 11. Calculated and fitted effective transfer rates as a function of temperature for sample A-$W3$ (350/9 nm).

height is lower than the average so that the transfer is easier at those places. The barrier height fluctuation could be as large as the inhomogeneous linewidth: e.g., 5 meV for the 9-nm QW.

In the above calculation and previous discussion of transfer, it has been assumed that excitons in the interwire region have a uniform spatial distribution. The laser spot is much larger than the interwire spacing, so that the generation rate of excitons is uniform, but the finite diffusion rate in the interwire region can, in principle, produce a nonuniform distribution. The time for an exciton to diffuse a distance L is $\sim L^2/4D$, where D is the diffusion constant, with a typical value 10 cm^2/s for free excitons and less than 1 cm^2/s for localized excitons in a quantum well[52] at low temperature ($\sim$4 K). For the widest wires the exciton is at most 1 μm from the wire, so the related diffusion time for free excitons is $\sim$200 ps, which is of the order of, but less than, the exciton lifetime. Thus even in this extreme case diffusion of free excitons can be taken to be fast and the distribution uniform. For smaller structures the diffusion time will be much shorter than the exciton lifetime. At low temperature the thermalized excitons are localized and D is very small. However transfer to the wire is very slow, so the exciton density is determined by radiative decay and the distribution is again uniform, except perhaps near the "low spots" in the barrier mentioned in the previous paragraph. Only in these spots may some depletion by transfer occur. However, diffusion is probably negligible so that only that a small number of excitons, whose wave functions actually overlap the barrier at these two spots are involved. For these reasons, we believe that spatial nonuniformity is not significant, and a kinetic model, which treats each group of excitons as a homogeneous population, is valid in both temperature regimes.

We will now develop a kinetic model to explain the activation and tunneling transfers quantitatively. First, we consider the situation in which both well and wire luminescence is dominated by free-exciton recombination. Two kinetic equations can be written down for the excitons in the interwire region and the wires, respectively:

$$\frac{dN_1}{dt}=g_1-N_1(w_t+w_1)\ , \tag{5}$$

$$\frac{dN_2}{dt}=g_2+N_1w_t-N_2w_2\ , \tag{6}$$

where N_1 and N_2 are the numbers of excitons per unit wire length near the band edge in the interwire region and in the wires, respectively, g_1 and g_2 are the corresponding exciton generation rates: g_2 includes contributions both from direct excitation and from capture transfer, w_t is the transfer rate defined above, w_1 is the decay rate of the QW excitons in the absence of transfer and w_2 is the decay rate of the QWW excitons. Nonradiative decay is ignored, as is reverse transfer from the wire to well, since the depth of the potential well is much greater than k_BT and energy relaxation within the wire is fast. Solving (5) and (6), we find for the steady-state luminescence from the well (I_1) and from the wire (I_2):

$$I_1=w_1N_1=\frac{g_1}{1+w_t/w_1}\ , \tag{7}$$

$$I_2=w_2N_2=g_2+\frac{g_1}{1+w_1/w_t}\ . \tag{8}$$

These simple results must be modified to allow for exciton localization. Figure 12 shows the kinetic model to be used. Let N_1 and N_{1t} be the numbers of free and localized excitons in the well, respectively, and N_2 and N_{2l} the numbers of free and localized excitons in the wire. There are now four kinetic equations for the exciton densities, as follows:

$$\frac{dN_1}{dt}=g_1-N_1(w_t+w_1+w_{1fl})+N_{1l}w_{1lf}\ , \tag{9}$$

$$\frac{dN_{1l}}{dt}=N_1w_{1fl}-N_{1l}(w_{1l}+w_{1lf})\ , \tag{10}$$

$$\frac{dN_2}{dt}=g_2+N_1w_t-N_2(w_2+w_{2fl})+N_{2l}w_{2lf}\ , \tag{11}$$

$$\frac{dN_{2l}}{dt}=N_2w_{2fl}-N_{2l}(w_{2l}+w_{2lf})\ , \tag{12}$$

where the w's are transition rates defined in Fig. 12, with subscript f standing for free excitons, l for localized excitons. In these equations, it has been assumed that localized excitons in the well region do not transfer to the wire directly, but can be thermally excited to a free-exciton state and then transfer to the wire. The solutions of (9)–(12) give the wire luminescence,

$$I_2=g_2+\frac{g_1}{1+f(T)}\ , \tag{13}$$

and the well luminescence,

$$I_1=\frac{g_1}{1+1/f(T)}\ , \tag{14}$$

where

$$f(T)=\frac{w_1+w_{1l}w_{1fl}/(w_{1l}+w_{1lf})}{w_t}\equiv\frac{w_1+w_{1l}N_{1l}/N_1}{w_t}\ . \tag{15}$$

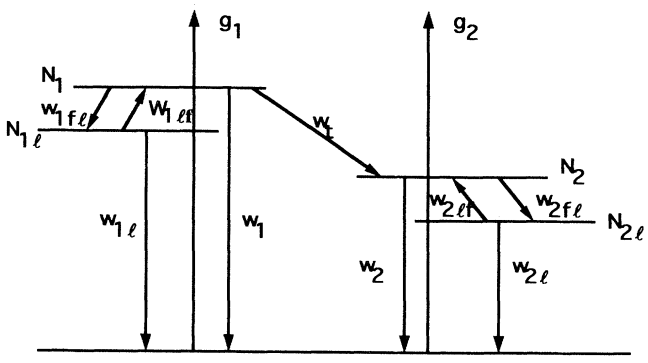

FIG. 12. Kinetic model showing exciton generation, transfer, relaxation, thermalization, and recombination in a quantum wire.

Note that I_1 and I_2 include the contributions of both free and localized excitons. $f(T)$ includes the contributions of three mechanisms: the thermally enhanced transfer rate w_t, the thermally prolonged free-exciton decay time $1/w_1$, and thermal delocalization of localized excitons described by w_{1lf}. The transfer is reduced by localization. There are too many parameters for a meaningful fit to the experimental data to (13) and (14). However, if we assume that free and localized excitons in the quantum well are in thermal equilibrium, we have $N_1/N_{1l}=c_1 T\exp(-E_{\rm loc}/k_B T)$,[58] where c_1 is a constant which depends on the density of localized states. Furthermore, we assume that $(w_1 N_1)/(w_{1l}N_{1l})\ll 1$, which is valid in these QW's as long as the temperature is not too high,[38] and we ignore the small tunneling transfer rate at the low-temperature limit. Writing the temperature-dependent transfer rate as $w_t=b\sqrt{T}\exp(V_0/k_B T)$, where b is a constant, we have

$$f(T)\approx AT^{-3/2}\exp(E/k_B T)\ , \tag{16}$$

where $A=w_{1l}/(bc_1)$, $E=E_{\rm loc}+V_0$. As an example, we apply (13) with $f(T)$ given by (16) to the experimental result shown in Fig. 6(a) for $W3$ (350/9 nm). Only data points below 55 K are fitted, since above this temperature nonradiative decay is significant, as shown by Fig. 8. The fitting parameters are $g_1=1.88$, $g_2=1.22$, $A=65.4\ \mathrm{K}^{3/2}$ and $E=5.6$ meV. With $w_{1l}=1/\tau_{\rm loc}=3.30\times10^9\ \mathrm{sec}^{-1}$, $c_1=0.0976\ \mathrm{K}^{-1}$, and $E_{\rm loc}=2.2$ meV from the study of the temperature dependence of the exciton decay time,[48] we find $w_t=b\sqrt{T}\exp(-V_0/k_B T)$, with $b=5.2\times10^8\ \mathrm{K}^{-1/2}\ \mathrm{sec}^{-1}$ and $V_0=3.4$ meV. The fitted curves are the full lines in Fig. 6(a). The curve for the wire luminescence agrees well with the data (filled circles). For the well luminescence, the predicted intensity is consistently lower than that observed (open circles), since some excitons are unavoidably created outside the patterned region by imperfectly focused and scattered laser light. The fitted ratio $g_2/g_1=0.65$ is larger than the geometric ratio 0.21, because of capture transfer. The value of w_t is reasonable in order of magnitude, compared to the high temperature results as shown in Fig. 11. However, V_0 is lower than the calculated barrier height $\sim$9 meV for the exciton by a factor 2.6. This discrepancy could perhaps be due to fluctuations in the barrier height, but it is more likely that the calculated stress pattern is inaccurate at the edges of the stressor, which may not be as sharply defined as assumed in the model.[28]

V. SUMMARY AND CONCLUSIONS

We have shown that strain-confined quantum wires and quantum dots have as high a luminescent efficiency at low temperature as unpatterned quantum wells, and retain this efficiency to significantly higher temperature. As the dimensionality of the nanostructures is reduced, nonradiative processes are efficiently suppressed.

Exciton transfer from quasi-two-dimensional regions to quasi-one-dimensional or quasi-zero-dimensional regions has been studied in strain-confined quantum wires and quantum dots. The transfer has three contributions: capture of hot excitons, tunneling, and classical activation, and is strongly temperature dependent. The thermally enhanced transfer is responsible for maintaining high luminescent efficiency at high temperature. The barrier to activated transfer is considerably lower than the theoretical prediction, probably because it is difficult to calculate the precise stress distribution at the edge of the stressor. Exciton localization, due to the fluctuations of quantum-well thickness and wire or dot width, plays an important role in determining the temperature dependence of the luminescent intensity, luminescent decay time, and exciton transfer in these quantum wire and dot structures up to at least 80 K.

ACKNOWLEDGMENTS

We are grateful to Professor Weikun Ge for helpful discussions. This work was supported in part by the Office of Naval Research under Grant No. N001491J429.

*Present address: NREL, 1617 Cole Blvd., Golden, CO 80401.

[1]See *Semiconductor Quantum Wells and Superlattices: Physics and Applications,* edited by D. S. Chemla and A. Pinczuk, special issue of IEEE J. Quantum Electron. **QE-22**, 9 (1986); *Optical Properties of Semiconducting Quantum Wells and Superlattices,* edited by M. D. Sturge and M.-H. Meynadier, special issue of J. Lumin. **44**, 4 (1989).

[2]H. Sakaki, Jpn. J. Appl. Phys. **19**, 94 (1980).

[3]K. Kash, J. Lumin. **46**, 69 (1990).

[4]M. Kohl, D. Heitmann, P. Grambow, and K. Ploog, Phys. Rev. Lett. **63**, 2124 (1989).

[5]B. I. Miller, A. Shahar, U. Koren, and P. I. Corvini, Appl. Phys. Lett. **54**, 188 (1989).

[6]G. Mayer, F. E. Prins, G. Lehr, H. Schweizer, H. Leier, B. E. Maile, J. Straka, A. Forchel, and G. Weimann, Phys. Rev. B **47**, 4060 (1993).

[7]E. Kapon, D. M. Hwang, and R. Bhat, Phys. Rev. Lett. **63**, 430 (1989).

[8]K. Kash, J. M. Worlock, M. D. Sturge, P. Grabbe, J. P. Harbison, A. Scherer, and P. S. D. Lin, Appl. Phys. Lett. **53**, 782 (1988).

[9]Z. Xu and P. M. Petroff, J. Appl. Phys. **69**, 6564 (1991).

[10]K. K. Cheng, K. C. Hsieh, and J. N. Baillargeon, Appl. Phys. Lett. **60**, 2892 (1992).

[11]K. H. Ploog, P. Nötzel, and M. Ilg, J. Vac. Sci. Technol. B **11**, 1675 (1993).

[12]J. M. Moison, F. Houzay, F. Barthe, L. Leprince, E. André, and O. Vatel, Appl. Phys. Lett. **64**, 196 (1994).

[13]D. Leonard. M. Krishnamaurthy, C. M. Reaves, S. P. Denbaars, and P. M. Petroff, Appl. Phys. Lett. **63**, 3203 (1994).

[14]H. Lage, D. Heitmann, R. Cingolani, P. Grambow, and K. Ploog, Phys. Rev. B **44**, 6550 (1991).

[15]Y. Hirayama, S. Taruchu, Y. Suzuki, and H. Okamoto, Phys. Rev. B **37**, 2774 (1988).

[16]I.-Hsing Tan, D. Lishan, R. Mirin, V. Jayaraman, T. Yasuda, E. Hu, and J. Bowers, Appl. Phys. Lett. **59**, 1875 (1991).

[17]K. Kash, B. P. Van der Gaag, Derek D. Mahoney, A. S. Gozdz, L. T. Florez, J. P. Harbison, and M. D. Sturge, Phys. Rev. Lett. **67**, 1326 (1991).
[18]I.-H. Tan, D. Lishan, R. Mirin, V. Jayaraman, T. Yasuda, E. L. Hu, and J. Bowers, Appl. Phys. Lett. **59**, 1875 (1991).
[19]K. Kash, Derek D. Mahoney, B. P. Van der Gaag, A. S. Gozdz, J. P. Harbison, and L. T. Florez, J. Vac. Sci. Technol. B **10**, 2030 (1992).
[20]I.-H. Tan, R. Mirin, V. Jayaraman, S. Shi, E. L. Hu, and J. Bowers, Appl. Phys. Lett. **61**, 300 (1992).
[21]M. Oestreich, W. W. Rühle, H. Lage, D. Heitmann, and K. Ploog, Phys. Rev. Lett. **70**, 1682 (1993).
[22]G. Mayer, F. E. Prins, G. Lehr, H. Schweizer, H. Leier, B. E. Maile, J. Straka, A. Forchel, and G. Weimann, Phys. Rev. B **47**, 4060 (1993).
[23]J. Christen, M. Grundmann, E. Kapon, E. Colas, D. M. Hwang, and D. Bimberg, Appl. Phys. Lett. **61**, 67 (1992).
[24]I.-H. Tan, T. Yasuda, Y.-L. Chang, R. Mirin, E. L. Hu, Y. Segawa, J. Bowers, and J. L. Merz, Appl. Phys. Lett. **62**, 1378 (1993).
[25]R. Cingolani, R. Rindaldi, M. Ferrara, G. C. La Rocca, H. Lage, D. Heitmann, K. Ploog, and H. Kalt, Phys. Rev. B **48**, 14 331 (1993).
[26]H. Kalt, J. Lumin. **60/61**, 262 (1994).
[27]M. Kohl, D. Heitmann, P. Grambow, and K. Ploog, Phys. Rev. Lett. **63**, 2124 (1989).
[28]K. Kash, J. M. Worlock, A. S. Gozdz. B. P. Van der Gaag, J. P. Harbison, P. S. D. Lin, and L. T. Florez, Surf. Sci. **229**, 245 (1990).
[29]Yong Zhang, M. D. Sturge, K. Kash, J. Yater, B. P. Van der Gaag, A. S. Gozdz, L. T. Florez, and J. P. Harbison, Bull. Am. Phys. Soc. **38**, 393 (1993).
[30]Yong Zhang, M. D. Sturge, K. Kash, B. P. Van der Gaag, A. S. Gozdz, L. T. Florez, and J. P. Harbison, J. Lumin. **60/61**, 400 (1994).
[31]G. Wang, S. Fafard, D. Leonard, J. E. Bowers, J. L. Merz, and P. M. Petroff, Appl. Phys. Lett. **64**, 2815 (1994).
[32]K. Kash, J. M. Worlock, Derek D. Mahoney, A. S. Gozdz, B. P. Van der Gaag, J. P. Harbison, P. S. D. Lin, and L. T. Florez, Surf. Sci. **228**, 415 (1990).
[33]Yong Zhang, Phys. Rev. B **49**, 14 352 (1994).
[34]C. Weisbuch, R. Dingle, A.C. Gossard, and W. Wiegmann, Solid State Commun. **38**, 709 (1981).
[35]J. Martinez-Pastor, A. Vinattieri, L. Carraresi, M. Colocci, Ph. Roussignol, and G. Weimann, Phys. Rev. B **47**, 10 456 (1993).
[36]Yong Zhang, Yitong Gu, M. D. Sturge, K. Kash, B. P. Van der Gaag, A. S. Gozdz, L. T. Florez, and J. P. Harbison (unpublished).
[37]Because the dielectric constant of the carbon layer is between that of air and the semiconductor, one might expect that more light will be coupled into the semiconductor under the stressor, especially when the thickness of the stressor is close to one-quarter of the laser wavelength in the carbon. This "antireflection" effect can be roughly estimated by using the plane-wave approximation even though the lateral extent of the stressor is comparable to the light wavelength. For example, if we take $n=1.82$ for glassy carbon and $n=3.86$ for GaAs of 632.8 nm, the reflection coefficient is reduced from 0.35 to 0.32 by a 160-nm-thick carbon layer, and to 0.03 by a 100-nm layer. If absorption in the carbon layer can be neglected (a doubtful assumption), this "antireflection" effect might be expected to increase the effective geometric ratio of sample *A* by 5% and of sample *B* by 40%, and thus might be significant for sample *B*. Diffraction at the edges of the stressor will also alter the coupling of the radiation into and out of the wire. However, the external quantum efficiency of the patterned region is the same as that of the unpatterned, which would be an unlikely coincidence if the coupling efficiency were appreciably different, so we have ignored this complication.
[38]Yong Zhang, Ph.D. thesis, Dartmouth College, 1994.
[39]U. Bockelmann and G. Bastard, Phys. Rev. B **42**, 8947 (1990).
[40]H. Benisty, C. M. Sotomayor-Torrès, and C. Weisbuch, Phys. Rev. B **44**, 10 945 (1991).
[41]M. Kohl, D. Heitmann, W. W. Ruhle, P. Grambow, and K. Ploog, *ibid.* **41**, 12 338 (1990).
[42]J. N. Patillon, C. Jay, M. Iost, R. Gamonal, J. P. Andrè, B. Soucail, C. Delalande, and M. Voos, Superlatt. Microstruct. **8**, 335 (1990).
[43]M. Notami, M. Naganuma, T. Nishida, T. Tamamura, H. Iwamura, S. Nojima, and M. Okamoto, Appl. Phys. Lett. **58**, 720 (1991).
[44]H. Leier, A. Forchel, B. E. Maile, G. Mayer, J. Hommel, G. Weimann, and W. Schlapp, Appl. Phys. Lett. **56**, 48 (1989).
[45]E. M. Clausen, H. G. Craighead, J. M. Worlock, J. P. Harbison, L. M. Schiavone, L. T. Florez, and B. P. Van der Gaag, Appl. Phys. Lett. **55**, 1427 (1989).
[46]G. Mayer, B. E. Maile, R. Germann, A. Forchel, P. Grambow, and H. P. Meier, Appl. Phys. Lett. **56**, 2016 (1990).
[47]Garnett W. Bryant, Bull. Am. Phys. Soc. **37**, 80 (1992).
[48]Yong Zhang, M. D. Sturge, K. Kash, B. P. Van der Gaag, A. S. Gozdz, L. T. Florez, and J. P. Harbison (unpublished).
[49]E. M. Gyorgy, R. C. Le Craw, and M. D. Sturge, J. Appl. Phys. **37**, 1303 (1966).
[50]E. H. Rhoderick and R. H. Williams, *Metal-Semiconductor Contacts*, 2nd ed. (Clarendon, Oxford, 1988), p. 89.
[51]D. Bohm, *Quantum Theory* (Dover, New York, 1989), p. 286.
[52]J. Hegarty and M. D. Sturge, J. Opt. Soc. Am. B **2**, 1143 (1985).
[53]D. J. Wolford, G. D. Gilliland, T. F. Kuech, J. A. Bradley, and H. P. Hjalmarson, Phys. Rev. B **47**, 15 601 (1993).
[54]R. Zimmermann, Phys. Status Solidi B **173**, 129 (1992).
[55]K. Kash, B. P. Van der Gaag, J. M. Worlock, A. S. Gozdz, D. D. Mahoney, J. P. Harbison, and L. T. Florez, in *Localization and Confinement of Electrons in Semiconductors*, edited by F. Kuchar, H. Heinrich, and G. Bauer (Springer-Verlag, Berlin, 1990), p. 39.
[56]H. Tuffigo, R. T. Cox, G. Lentz, N. Magnea, and H. Mariette, J. Cryst. Growth **101**, 778 (1990).
[57]G. Bastard, *Wave Mechanics Applied to Semiconductor Heterostructures* (Les Éditions de Physique, Les Ulis Cedex, 1988), p. 110.
[58]D. S. Citrin, Phys. Rev. B **47**, 3832 (1993).